Characterization of Mechanically Attrited Si/SiO_x Nanoparticles and Their Self-Assembled Composite Films

Thomas Phely-Bobin, Debjit Chattopadhyay, and Fotios Papadimitrakopoulos*

Nanomaterials Optoelectronics Laboratory, Department of Chemistry, Polymer Program, Institute of Materials Science, University of Connecticut, Storrs, Connecticut 06269-3136

Received June 7, 2001

The surface chemistry and structure of nanosized silicon, as obtained by high-energy ball milling and its subsequent dispersion in ethanol, via sonication-assisted oxidation, is presently described. These Si/SiO_x suspensions that spontaneously assemble on glass surfaces were investigated as a function of pH in a variety of oxidizing agents and atmospheres. Spectroscopic characterization indicates that at pH 5 or below and in the absence of H_2O, the Si−OEt groups present on the surface of these nanoparticles get protonated, providing the driving force to assemble on less positively charged glass substrates. X-ray photoelectron spectroscopy concurs with a core/shell (Si/SiO_x) nanoparticle structure, with an average Si-atom ratio of 45/55 and x in the order of 1.5. In addition, Raman investigation suggests that the Si core in these nanoparticles (45% of the total Si-atom content) is composed of crystalline (34%) and amorphous (11%) parts.

Introduction

Nanosized silicon has attracted considerable interest for applications in microelectronics,[1−3] optoelectronics,[4] photonics,[5−10] and hybrid composite materials.[11−13] The high refractive index and low absorption coefficient of crystalline silicon[14] renders it suitable for manufacturing photonic band gap (PBG) structures.[8,15−17] Recently, our laboratory reported a method for the preparation of colloidal suspensions of Si nanoparticles and nanocomposites with refractive index as high as 3.2 and increased transparency in the red part of the visible spectrum.[18] With an average size of 20 nm and size distribution of 25%, these particles are large enough to have refractive index as high as bulk Si[19] and small enough to exhibit a blue shifted absorption due to Mie scattering and local field effects.[18,20] Moreover, since these particles are smaller than 1/10 of the wavelength of the transmitted light, Rayleigh scattering can be minimized assuming that no agglomeration takes place.[21] Self-assembly of nanosized Si could potentially ease the fabrication of high refractive index nanocomposites as well as complex three-dimensional periodic structures for PBG applications. The controllable growth of SiO_x coatings on these nanoparticles, via a sonication-assisted oxidation process, provides an effective avenue for passivation/cladding, along with the ability to perform siloxane-based chemistry for further surface modification.[22] Tetraethoxysilane (TEOS), a byproduct of the sonication-assisted oxidation, was shown to be crucial for the growth of self-assembled films with suppressed scattering.[22] This paper sheds more light on the fabrication and structural composition of these Si/SiO_x core/shell nanoparticles along with an in-depth understanding of the surface chemistry that drives their self-directed assembly on glass substrates.

* To whom correspondence should be addressed. Tel: (860)-486-3447. Fax: (860)-486-4745. E-mail: papadim@mail.ims.uconn.edu.

(1) Wu, W.; Huang, X.; Chen, K.; Xu, J. B.; Gao, X.; Xu, J.; Li, W. *J. Non-Cryst. Solids* **1998**, *227−230*, 1045−8.
(2) Kim, D. W.; Lym, S. H.; Jung, M. Y.; Jeon, H. T.; Choi, S. S. *Microelectron. Eng.* **1999**, *46*, 423−6.
(3) Piatkowska, A.; Gawlik, G.; Jagielski, J. *Appl. Surf. Sci.* **1999**, *141*, 333−8.
(4) Soref, R. *MRS Bull.* **1998**, *23*, 20−4.
(5) Yablonovitch, E. *Phys. Rev. Lett.* **1987**, *58*, 2059−2062.
(6) John, S. *Phys. Rev. Lett.* **1987**, *58*, 2486−2489.
(7) Joannopoulos, J.; Meade, R.; Winn, J. *Photonic Crystals*; Princeton Press: Princeton, NJ, 1995.
(8) Blanco, A.; Chomski, E.; Grabtchak, S.; Ibisate, M.; John, S.; Leonard, S. W.; Lopez, C.; Meseguer, F.; Miguez, H.; Mondia, J. P.; Ozin, G. A.; Toader, O.; Driel, H. M. V. *Nature* **2000**, *405*, 437−440.
(9) Kawakami, S.; Kawashima, T.; Sato, T. *Appl. Phys. Lett.* **1999**, *74*, 463−465.
(10) Hanaizumi, O.; Ohtera, Y.; Sato, T.; Kawakami, S. *Appl. Phys. Lett.* **1999**, *74*, 777−9.
(11) Klabunde, K. J. *Free Atoms, Clusters, and Nanoscale Particles*; Academic Press: New York, 1994.
(12) Moser, W. R. *Advanced catalysts and nanostructured materials: modern synthetic methods*; Academic Press: New York, 1996.
(13) Hoch, H. C.; Jelinski, L. W.; Craighead, H. G. *Nanofabrication and biosystems: integrating materials science, engineering and biology*; Cambridge University Press: Cambridge, U.K., 1996.
(14) Palik, E. D. *Handbook of Optical Constants of Solids*; Academic Press: New York, 1985.
(15) Joannopoulos, J. D.; Villeneuve, P. R.; Fan, S. *Nature* **1997**, *386*, 143−149.
(16) Busch, K.; John, S. *Phys. Rev. Lett.* **1999**, *83*, 967−970.
(17) Yablonovitch, E. *Nature* **1999**, *401*, 539−541.
(18) Papadimitrakopoulos, F.; Wisniecki, P.; Bhagwagar, D. E. *Chem. Mater.* **1997**, *9*, 2928.
(19) Kyprianidou-Leodidou, T.; Caseri, W.; Suter, U. W. *J. Phys. Chem.* **1994**, *98*, 8992.
(20) Xie, Y. H.; Hybertsen, M. S.; Wilson, W. L.; Ipri, S. A.; Carver, G. E.; Brown, W. L.; Dons, E.; Weir, B. E.; Kortan, A. R.; Watson, G. P.; Liddle, A. J. *Phys. Rev. B* **1994**, *49*, 5386.
(21) Ogawa, T.; Kanemitsu, Y. *Optical properties of low-dimensional materials*; World Scientific: New York, 1995.
(22) Papadimitrakopoulos, F.; Phely-Bobin, T.; Wisniecki, P. *Chem. Mater.* **1999**, *11*, 522−525.

10.1021/cm010362l CCC: $22.00
Published on Web 03/01/2002

Experimental Section

Preparation of Colloidal Silicon Suspensions. The high-energy milling process used to prepare nanosized silicon has been described elsewhere.[18,23] After a 5 h milling process, the steel vial was unloaded and stored in an oxygen- and moisture-free glovebox. A portion of 200 mg of the nanomilled Si powder was placed in polypropylene containers and sonicated (using a Fisher Scientific FS9 ultrasonic cleaning bath) overnight in a mixture of 75 mL of ethanol (100%) and 8.6×10^{-7} mole of oxidizing agent (either benzoyl peroxide, dicumyl peroxide, peracidic acid, or 3-chloroperbenzoic acid). During the sonication, the atmosphere was carefully controlled with ca. 1.5 atm positive pressure (with a gas of choice). The sonicated suspension was then centrifuged at 3000 rpm for 90 min in a Sorvall Superspeed RC2−B centrifuge at room temperature. The supernatant liquid, containing the colloidal nanosilicon, was carefully removed and stored in sealed glass containers, to be later characterized based on the nature of oxidizing agent and surrounding atmosphere (either air, oxygen, argon, or nitrogen).

The pHs of the ethanolic suspensions of Si nanoparticles were measured with an Accumet 1001 Fischer Scientific pH meter equipped with a standard size porous glass electrode and an internal Ag/AgCl reference.

Characterization Techniques. Glass or quartz substrates were cleaned using piranha solution (7:3 H_2SO_4/H_2O_2) followed by copious rinsing in deionized H_2O, dried with compressed air, and stored in ethanol (100%). A Denton model DV-502A was used to thermally evaporate gold or silver on glass substrates operating at pressures below 10^{-6} Torr. To improve adhesion of gold on glass, a chromium-pretreated glass was used as a substrate for the evaporation of gold.

UV−vis spectra were recorded on a Perkin-Elmer Lambda 3840 array spectrophotometer. The pH of the as-obtained Si/SiO_x ethanolic suspension after the sonication/oxidation process with benzoyl peroxide was 5.5. Successive centrifugation (10 000 rpm), decantation, and refilling with fresh ethanol were used to raise the pH of the ethanolic suspension of Si/SiO_x nanoparticles from 5.5 to 7.8. Seventeen glass vials were filled with equal volumes of nanosilicon colloid suspension, adjusted to different pHs by adding benzoic acid, and the suspensions were sealed and left standing at room temperature (25 °C) for 12 h. The pHs of the remaining 16 suspensions were lowered by addition of various amounts of benzoic acid. By the utilization of a custom built vial holder, the room-temperature absorption spectra of the central part of these vials were collected against a background of a similar sealed vial filled with ethanol.

Fourier transform IR (FTIR) spectroscopy data was obtained from a Nicolet Magna 560 using a TeGeSe detector with 4 cm^{-1} resolution. Thin films of Si nanoparticles were deposited or assembled on double polished Si wafer, coated on both sides with ca. 400 Å of thermally grown silicon oxide (using dry O_2 at 900 °C for 20 min) and held at an angle of 45° with respect to the incident IR beam. This increases the sampling path length and eliminates the interference fringes from the double polished silicon wafer. A minimum of 128 scans were signal averaged, and the background, consisting of double polished Si wafers and air, was carefully subtracted from the sample's spectra.

Raman spectra were recorded on a Renishaw Ramanoscope system equipped with a microscope, in which the laser spot size could be focused to be as small as 1 μm in diameter (×100 objective), and power output of 35 mW. The Raman spectra were collected using a 514.5 nm excitation argon ion laser. The instrument was calibrated using high-purity single crystal (100) Si. Samples of the starting polycrystalline Si powder were of 99.5% nominal purity; the as-milled Si and the self-assembled Si/SiO_x nanoparticles were cast or assembled on glass substrates that were previously covered with gold (thickness higher than 130 nm). Both crystalline Si (c-Si) and amorphous Si (a-Si) Raman peaks were well fitted with Gaussian−Lorentzian functions.

Table 1. Effect of Oxidative Agents as a Function of pH and Surrounding Atmosphere to the Preparation of Metastable Si/SiO_x Nanoparticle Suspension. MS Refers to Obtaining Metastable Suspensions, Which Self-Assembled on Glass Substrates. "—" Refers to Obtaining No Suspension (i.e., the nanoparticles remained aggregated and quickly precipitated out)

oxidizing agent	suspension pH[a]	atmosphere			
		oxygen	argon	nitrogen	air
benzoyl peroxide	pH < 5	MS	—	—	MS
peracidic acid	pH < 4	—	—	—	—
dicumyl peroxide	pH > 7	—	—	—	—
dicumyl peroxide	pH < 4[b]	MS	—	—	MS
3-chloroperbenzoic acid	pH < 5	MS	—	—	MS

[a] pH obtained after sonication, unless otherwise noted. [b] pH was lowered to below 4 by bubbling HCl.

Table 2. Energy Positions, fwhm's, and Percentage of Total Area for Si^0 and Various Suboxides as Determined by Fitting the Si 2p XPS Spectrum Shown in Figure 2

	energy[a] (eV)	fwhm (eV)	% of total area
Si^0	0	1.2	43.9
Si^{1+}	0.87	0.8	8.3
Si^{2+}	1.81	1.1	4.7
Si^{3+}	2.95	1.4	18.4
Si^{4+}	3.92	1.5	24.7

[a] The energy positions of various suboxides are reported with their offset relative to that of Si^0 at 99.07 eV.

Gas chromatography and mass spectroscopy (GC/MS) analyses were performed using a HP 6890 series GC system and a HP 6890 series mass selective detector.

X-ray photoelectron spectroscopy (XPS) data was obtained on a PHI ESCA 5300 X-ray photoelectron spectrometer, equipped with a monochromatic Al Kα anode X-ray source (1486.4 eV) and hemispherical analyzer. The photoelectron takeoff angle was set at 62°. Binding energies were corrected from static charging of the samples by referring them to the C (1s) peak arising from airborne carbon contamination at 284.6 eV. To avoid contribution from glass or SiO_x-coated Si substrate, the self-assembly of Si/SiO_x nanoparticles was performed on a silver-coated glass substrate. The as-milled silicon samples were stored in a glovebox under positive pressure of nitrogen and transferred to the antichamber of the XPS apparatus using a specialized vacuum jacket unit that ensures minimal contamination during the transfer process. The Si^0, Si^{1+}, Si^{2+}, Si^{3+}, and Si^{4+} components were fitted with Gaussian−Lorentzian function. The energy positions of the deconvoluted peaks were constrained to values approximately 10% off those previously reported (see Table 2).[24,25] To accurately fit the different peaks, the full width at half-maximums (fwhm's) were allowed to vary from 15 to 40% off the values previously reported.[26]

Results

XPS is particularly suitable for the study of nonstoichiometric silicon oxide thin films and nanoparticles[27] and was utilized to determine the relative amount of SiO_2 and other suboxides on the surface of these silicon

(23) Papadimitrakopoulos, F.; Phely-Bobin, T.; Wisniecki, P. *Am. Chem. Soc., Div. Polym. Chem.* **1998**, *39*, 177.

(24) Himpsel, F. J.; McFeely, F. R.; Taleb-Ibrahimi, A.; Yarmoff, J. A. *Phys. Rev. B* **1988**, *38*, 6084.

(25) Niwano, M.; Katakura, H.; Takakuwa, Y.; Miyamoto, N. *J. Appl. Phys.* **1990**, *68*, 5576.

(26) Grunthaner, P. J.; Hecht, M. H.; Grunthaner, F. J. *J. Appl. Phys.* **1987**, *61*, 629.

(27) Hartstein, A.; Tsang, J. C.; DiMaria, D. J.; Dong, D. W. *Appl. Phys. Lett.* **1980**, *36*, 836.

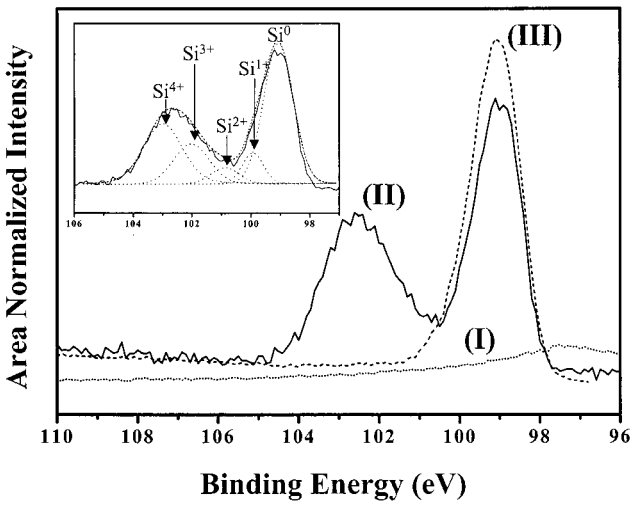

Figure 1. Detailed Si 2p XPS scans for as-milled nanosized silicon **(**III**)** (dashed line) and self-assembled Si/SiO_x nanoparticles **(**II**)** (solid line) on top of silver-coated glass substrates **(**I**)** (dotted line). The inset depicts the deconvolution of **(**II**)** to its various suboxide components.

nanoparticles during various stages of its chemical and physical modifications.

A detailed scan for Si 2p is shown in Figure 1. The dotted line (I) is for the bare silver-coated glass, which, as expected, exhibits a relatively flat background in the 96−110 eV region. The silver-coated glass substrate was immersed in an ethanolic suspension of Si/SiO_x nanoparticles for 3 h, and its XPS spectrum was recorded. The solid line (II) illustrates the XPS spectrum of this self-assembled film of Si/SiO_x nanoparticles, which closely resembles that of bare Si/SiO_x nanoparticles (not presently shown). The inset of Figure 1 illustrates the deconvolution of the SiO_x peak to its various suboxide components (e.g., Si^{1+} (Si_2O), Si^{2+} (SiO), Si^{3+} (Si_2O_3), and Si^{4+}), further elaborated in the Discussion.[28,29] The dashed line (III) illustrates the Si 2p spectrum of the as-milled silicon nanopowder. Particular care was taken to avoid exposure of the nanomilled Si to ambient (moisture and oxygen) environment. The presence of the strong Si^0 signal, peaking at 99.1 eV, and the lack of any detectable signal in the 101−104 eV region, characteristic of SiO_x species, signifies the successful exclusion of water and oxygen during the nanomilling and storage processes.

Figure 2 depicts the effect of pH on the stability of the suspension of Si/SiO_x nanoparticles. As the pH is lowered, the stability of the ethanolic Si/SiO_x dispersion points to the presence of three different regimes. In regime I (pH ranging from 7.8 to 6.7), the Si/SiO_x nanoparticles were found to be stable over a couple of years, showing neither agglomeration/precipitation nor adsorption onto the sidewalls of the vial. In regime II (pH ranging from 6.7 to 4.9), the nanoparticles formed large agglomerates that precipitated, leaving behind ethanol that does not absorb at 330 nm. In regime III (pH ranging from 4.9 to 3.8), the nanoparticles spontaneously adsorb on all glass surfaces. Due to adsorption of these nanoparticles onto the bottom as well as the sidewalls of the vial, the midlevel absorption is decreased by about 25%.

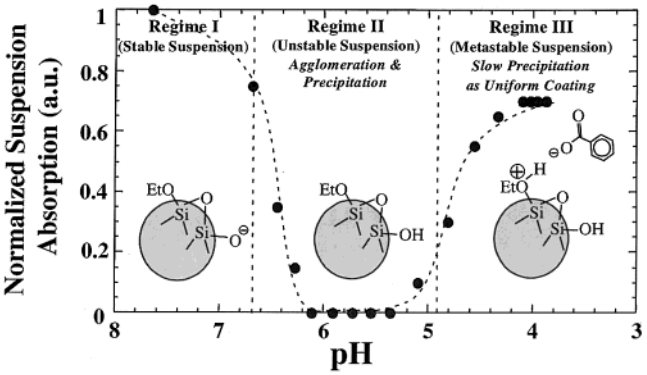

Figure 2. Normalized absorption for ethanolic Si/SiO_x suspensions as a function of pH. Suspension stability exhibits three distinct pH regimes (see text for details). Curve is drawn to guide the eye.

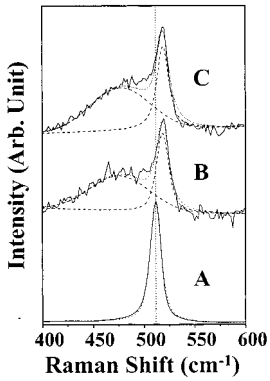

Figure 3. Detailed Si (c-Si due to the $q = 0$ transverse optical (TO) phonon modes and a-Si) Raman spectra of the starting polycrystalline Si powder (A), the as-milled nanosized silicon Si (B), and self-assembled Si/SiO_x nanoparticles (C) on gold substrates.

Raman spectroscopy has been shown to be a suitable technique for the study of different forms of Si. Qualitative[30−32] and quantitative[33,34] characterizations of thin films with polycrystalline and amorphous Si have been previously reported.[27,35] Figure 3 illustrates the Raman spectra of (A) the starting polycrystalline Si powder (99.5% nominal purity and 325 mesh size) as obtained from Alfa Aesar, (B) the as-milled Si nanopowder, and (C) the self-assembled Si/SiO_x nanoparticles from the ethanolic suspension (12 h) on gold substrates. The deconvolution of these Raman spectra to their polycrystalline and amorphous contents is further elaborated in the Discussion.

The relative contribution of the organic−inorganic chemical functionalities of these Si/SiO_x nanoparticles and their assemblies have been characterized by FTIR. Figure 4A depicts the FTIR spectrum of Si/SiO_x nanoparticles, deposited by drop casting and solvent evapo-

(28) Grunthaner, P. J.; Hecht, M. H.; Grunthaner, F. J.; Johnson, N. M. *J. Appl. Phys.* **1986**, *61*, 629.
(29) Hollinger, G.; Himpsel, F. J. *J. Vac. Sci. Technol., A* **1983**, *1*, 640.
(30) Kamiya, T.; Kishi, M.; Ushirokawa, A.; Katoda, T. *Appl. Phys. Lett.* **1981**, *38*, 377.
(31) Richter, H.; Ley, L. *J. Phys.* **1982**, *42*, 247.
(32) Iqbal, Z.; Veprek, S. *J. Phys. C: Solid State Phys.* **1982**, *15*, 377.
(33) Tsu, R.; Gonzalez-Hernandez, J.; Chao, S. S.; Lee, S. C.; Tanaka, K. *Appl. Phys. Lett.* **1982**, *40*, 534.
(34) Shimada, T.; Katayama, Y.; Nakagawa, K.; Matsubara, H.; Migitaka, M.; Maruyama, E. *J. Non-Cryst. Solids* **1983**, *59/60*, 783.
(35) Olego, D. J.; Baumgart, H. *J. Appl. Phys.* **1988**, *63*, 2669.

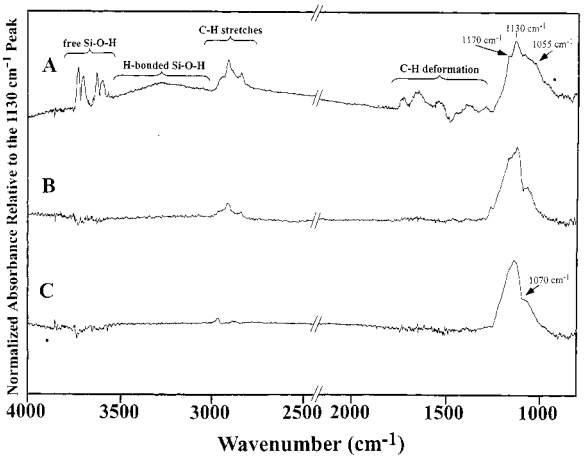

Figure 4. FTIR spectrum of neat Si/SiO$_x$ nanoparticles (A). FTIR spectra of Si/SiO$_x$ nanoparticle assemblies in the presence and absence of tetraethoxysilane (TEOS) (B and C, respectively) (see text for details).

ration on a double polished Si wafer, coated on both sides with ca. 400 Å of thermally grown SiO_2. Particular effort was taken to remove all solubilized reagents (benzoyl peroxide) and side products (TEOS, benzoic acid, and benzoylethylester) that originated from the sonication/oxidation process, prior to drop casting, using four successive cycles of centrifugation (10 000 rpm), supernatant decantation, and refilling with fresh ethanol. The presence and absence of TEOS, a byproduct of the sonication/oxidation process, has been argued to play an important role in this self-assembly process.[22] Figure 4B illustrates the FTIR spectrum of the Si/SiO$_x$ assemblies following a 12 h immersion in an ethanolic suspension of silicon nanoparticles (whose FTIR is shown in Figure 4A), where its pH was lowered to 4.7 using benzoic acid. This is compared to Figure 4C, which depicts the FTIR spectrum of a 12 h Si/SiO$_x$ assembled film, where the unreacted organic reagents and side products produced during the sonication/oxidation process (i.e., TEOS) were not removed.

Discussion

The formation of stable Si colloids in polar protic solvents (e.g., EtOH, MeOH, H_2O, etc.) has been attributed to the growth of an outer shell of a thin SiO$_x$ passivating layer.[18,22,36−38] The formation of "metastable" Si/SiO$_x$ nanoparticle suspensions (that are capable of self-assembling on a variety of substrates at pHs below 5.5) depends greatly on the chemical groups present on the surface and the extent of the ionization.[22] On the basis of the similar optical characteristics for both suspensions (isolated nanoparticles) and assemblies (densely packed nanoparticles), it is safe to conclude that the thickness of the SiO$_x$ coating adequately confines the exited state within the silicon core.[18,22] However, the transition from suspension to thin film dramatically reduces the scattering, as illustrated in Figure 5. It is presently believed that concentration fluctuations in the ethanolic suspension contribute to the increased scattering witnessed in cuvette A. In contrast, the self-assembled Si/SiO$_x$ films on the walls of cuvette B suppress scattering to an extent close to that of the reference cuvette C, filled with ethanol. As it will become apparent later on in the Discussion, the origin of the reduced scattering can in part be explained by the formation of a SiO$_x$ matrix around the Si/SiO$_x$ nanoparticles (as part of the slow hydrolysis and condensation of TEOS present in the metastable nanoparticle suspension).

The controlled oxidation of nanomilled Si powder in EtOH (100%, where moisture has been carefully excluded), in the presence of benzoyl peroxide, has been previously reported to yield such metastable Si/SiO$_x$ suspensions.[22] In this study, a variety of oxidative agents were investigated as a function of pH and surrounding atmosphere (see Table 1). Significantly, in both oxygen and dry air atmosphere, the formation of an orange metastable suspension of silicon nanoparticles occurs both in the presence of benzoyl peroxide and 3-chloroperbenzoic acid. The presence of oxygen turned out to be vital for this sonication-assisted oxidation process. Argon, nitrogen, and carbon dioxide atmospheres failed to yield metastable Si/SiO$_x$ suspensions, leaving behind largely agglomerated precipitates. Subsequent GC/MS characterization of the soluble organic reactants and byproducts, from benzoyl peroxide/oxygen combination, indicates the presence of benzoic acid, benzoylethylester, and TEOS, along with unreacted benzoyl peroxide.[22] Currently, the sonication-assisted cleavage of benzoyl peroxide is believed to activate oxygen,[39] followed by a cascade of events that lead to the slow surface oxidation of silicon nanoparticles. During this process, benzoyl and siloxy radicals interact with ethanol forming benzoylethylester, benzoic acid, TEOS, and H_2O. This process also functionalizes the surface of the nanoparticles with Si−OEt groups. The reason that these Si−OEt groups remain partially unhydrolyzed is attributed to the rapid consumption of generated H_2O in oxidizing Si (see Figure 4A). As evident from Figure 2, the pH for the formation of this metastable Si/SiO$_x$ nanoparticle suspension must be below 5.5. Since benzoic acid ($pK_a = 4.19$) is a relatively strong acid, generating small amounts of this compound can lower the pH to the desired value. Similarly, the strong acidities of 3-chloroperbenzoic acid ($pK_a = 3.98$) (oxidative agent) and the resulting byproduct, 3-chlorobenzoic acid ($pK_a = 3.82$), can lower both starting and ending pHs to below 5. In the case of dicumyl peroxide, the oxidative decomposition yields a tertiary alcohol whose acidity is well above that required to reach the desired pH. When HCl gas was bubbled into the ethanolic suspension to lower its pH below 4, the sonication-assisted oxidation process resulted in metastable Si/SiO$_x$ nanoparticle suspension. In the case of peracetic acid ($pK_a = 8.2$), 32% in solution in acetic acid ($pK_a = 4.75$), our failure to obtain metastable Si/SiO$_x$ suspensions is attributed to a significant amount of water present in this oxidizing mixture.

(36) Bhagwagar, D. E.; Wisniecki, P.; Papadimitrakopoulos, F. *Mater. Res. Soc. Symp. Ser.* **1997**, *457*, 439.
(37) Littau, K. A.; Szajowski, P. J.; Muller, A. J.; Kortan, A. R.; Brus, L. E. *J. Phys. Chem.* **1993**, *97*, 1224.
(38) Bley, R. A.; Kauzlarich, S. M.; Davis, J. E.; Lee, H. W. H. *Chem. Mater.* **1996**, *8*, 1881.
(39) Sheppard, C. S. *Peroxy Componds*; Mark, H. F., Bikales, N. M., Overberger, C. G., Mendes, G., Eds.; Wiley-Interscience: New York, 1988; Vol. 11, pp 1−21.

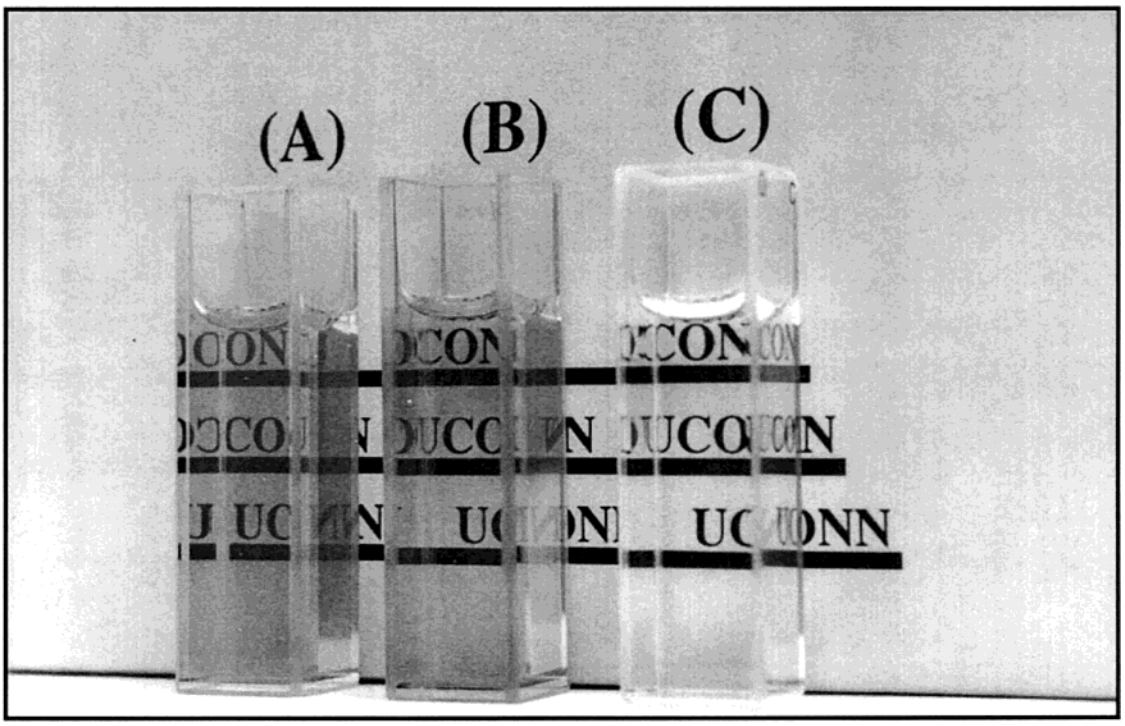

Figure 5. Optical appearance of an ethanolic suspension of Si/SiO_x nanoparticles before (A) and after (B) their self-assembly on the cuvette walls; (C) is a control cuvette, filled with ethanol (see text for details).

Figure 4A depicts the FTIR spectrum of silicon nanoparticles, subjected to successive centrifugation/decantation/resuspension cycles to remove all organic reactants and byproducts generated during their sonication-assisted oxidation process, raising the pH of this suspension to 7.8. The combination of sonication-assisted oxidation in ethanol followed by further H_2O-assisted Si oxidation[40] decorates the surface of these nanoparticles with Si−OEt, Si−OH, and Si−O−Si functionalities.[22] Starving the system of H_2O explains why Si−OEt does not hydrolyze to silanol (Si−OH) groups. The silanol (Si−OH) groups are witnessed as two doublets centered around 3712 and 3612 cm^{-1} (associated with non-hydrogen bonded Si−OH stretching) along with a much broader peak, centered around 3300 cm^{-1}, representing the hydrogen bonded Si−O−H stretching.[41−43] A strong absorption envelope of 1170−1150 cm^{-1} is due to Si−O−Si and Si−O−C stretching modes.[40,44] The ethoxysilane (SiOEt) characteristic absorptions are seen at the 1170 and 1055 cm^{-1} shoulders (1170 cm^{-1} for the CH_3 rocking absorption and 1055 cm^{-1} for the Si−O−Si stretching of $Si(OEt)_n$ (n = 1, 2, 3) groups).[44] The strong absorptions, associated with C−H stretching and C−H deformations, between 2975 and 2850 cm^{-1} are additional evidence for the presence of ethoxysilane groups at the surface of the Si nanoparticles.[43]

Figure 2 illustrates the behavior of these Si/SiO_x nanoparticles in the absence of TEOS in the solution. The pH of the Si/SiO_x ethanolic solution affects their behavior dramatically (as shown by the two transitions observed in the titration of Si/SiO_x nanoparticles by an ethanol-based HCl solution included in the Supporting Information). In regime I (pH = 7.8), the nanoparticles are negatively charged and stable over time. At this pH, the negative charge on the nanoparticles is due to the silanol ionization (Si−OH → $Si-O^- + H^+$) and lack of protonation for both Si−OH and Si−OEt groups decorating their surface. This negative charge keeps these nanoparticles in suspension and prevents them from adsorbing on glass surfaces due to electrostatic repulsion. The transition from regime I to II is observed at pH 6.60. At pHs between 6.2 and 5.2, charge neutralization for these Si/SiO_x colloids causes the fast agglomeration and subsequent precipitation. As the pH is lowered below 5 (regime III), these nanoparticles get resuspended and they are prone to spontaneously assemble on a variety of surfaces such as glass, gold, or silver. Below pH 5, the partial protonation of the ethoxysilane groups provides a positive surface charge, which contributes to the temporary stability of the suspension of these nanoparticles (see Figure 2, regime III).[45] In contrast, the weaker nucleophilicity of Si−OH and Si−O−Si groups (present at the surface of glass or quartz substrates) vs the Si−OEt groups (on the nanoparticles) (see Figure 4A) makes these substrates less prone to protonation at low pH. This provides sufficient attractive forces between substrate and protonated nanoparticles to bring them together in spatial proximity where silanol condensation can occur and immobilize the nanoparticles.

The pH of the ethanolic suspension influences not only the net charge on the surface of these nanoparticles

(40) Liao, W. S.; Lee, S. C. *J. Appl. Phys.* **1996**, *80*, 1171.
(41) Mawhinney, D. B.; Glass, J. A.; Yates, J. T. *J. Phys. Chem. B* **1997**, *101*, 1202.
(42) Hoffmann, P.; Knozinger, E. *Surf. Sci.* **1987**, *188*, 181−198.
(43) Tedder, L. L.; Lu, G.; Crowell, J. E. *J. Appl. Phys.* **1991**, *69*, 7037.
(44) Deshmukh, S. C.; Aydil, E. S. *J. Vac. Sci. Technol.* **1995**, *A 13*, 2355.
(45) Pohl, E. R.; Osterholtz, F. D. *Kinetics and Mechanism of Aqueous Hydrolysis and Condensation of Alkyltrialkoxysilanes*; Ishida, H., Kumar, G., Eds.; Plenum Press: New York, 1983; Vol. 27.

but also the processes of Si−OEt hydrolysis and Si−OH condensation.[45−47] At acidic pH, the hydrolysis of TEOS and the ethoxysilane groups on the nanoparticle surface tends to be faster than the condensation of the silanol groups to form silica.[46,47] Thus, the liberated H_2O, due to Si−OH condensation toward silica, is quickly used in the hydrolysis of nearby Si−OEt groups. This leads to a gradual formation of a silica network where the slow condensation yields high optical quality surrounding matrixes. The limiting reagent in this deposition process appears to be H_2O, since two condensing silanol groups produce one molecule of H_2O that can further hydrolyze one Si−OEt group to form one Si−OH. Silanol condensation between the nanoparticles and glass substrate provides the initial H_2O generation. As previously shown,[22] these assemblies do not grow to more than an average thickness of 40 nm (i.e., two nanoparticles) due to the lack of H_2O. The top layer of these assemblies consists mostly of bare nanoparticles, with a positive surface charge due to their protonated Si−OEt groups, thus preventing subsequent nanoparticle deposition. The exposing of these assemblies to moisture causes the hydrolysis of the Si−OEt groups and offers the ability to grow thicker films.

The adsorption characteristics of Si/SiO_x nanoparticles on SiO_x-coated silicon substrates were investigated in the presence and absence of TEOS (see C and B in Figure 4, respectively). The disappearance of non-hydrogen bonded and hydrogen bonded silanol absorption features are evident for both cases. However, the lack of TEOS causes only partial hydrolysis of Si−OEt groups, witnessed by the remaining C−H stretching ~2900 cm^{-1} absorbance, C−H deformation, and the shoulders at 1170 and 1055 cm^{-1}. In contrast, the presence of TEOS facilitates the nearly complete elimination of Si−OEt groups on the nanoparticles (see Figure 4C). TEOS is presently believed to assist in the formation of a SiO_x network surrounding these nanoparticles. FTIR spectroscopy can only indirectly infer the presence of the SiO_x network on top of the SiO_x nanosilicon shell by the sharpening of the Si−O−Si stretching mode witnessed between 1125 and 1139 cm^{-1}. However, the lack of a surrounding SiO_x network greatly weakens interparticle/substrate adhesion, leading to increased scattering and poorer mechanical properties.

The oxidation states of Si (Si^{n+} with $n = 1$, 2, 3, and 4) and their relative percentages were investigated with the help of XPS. At an incident angle of 62°, the X-ray depth penetration is only about 4−8 nm. With a mean particle diameter of 20 nm, the data presented below are expected to be slightly weighed toward the surface composition (i.e., SiO_x). The inset in Figure 1 presents the deconvolution curves for each oxide.[24,48] A least-squares fitting procedure was utilized to deconvolute the Si 2p photoemission. The Si^0 suboxides Si^{1+} (Si_2O), Si^{2+} (SiO), Si^{3+} (Si_2O_3), and Si^{4+} (SiO_2) were fitted using the Gaussian−Lorentzian model. Table 2 presents the energy position, fwhm, and relative percentage area for each component of the fit. Although our fwhm values are 15−40% greater than those reported for grown SiO_x on Si wafers,[26] they present the similar progressive increase in fwhm from Si^{1+} to Si^{3+} associated with increasing number of Si−O bonds around a given Si atom.[28]

Table 3. Area Values of Si^0 and Various Suboxides and Their Contributions to the Oxygen Content as Determined by Fitting the Si 2p XPS Spectrum Shown in Figure 2[a]

	area (ab. unit)	contribution to oxygen content	corrected area (ab. unit)
Si^+ (Si_2O)	95	1/2	48
Si^{2+} (SiO)	53	1	53
Si^{3+} (Si_2O_3)	211	3/2	316
Si^{4+} (SiO_2)	282	2	564
$Si^{n+} = Si^{1+} + Si^{2+} + Si^{3+} + Si^{4+}$	641	total contribution to oxygen	981
Si^0	502	0	

[a] $(1/2Si^+ + Si^{2+} + 3/2Si^{3+} + 2Si^{4+})/(Si^+ + Si^{2+} + Si^{3+} + Si^{4+}) = 981/641 \approx 1.5$. $Si^0/(Si^+ + Si^{2+} + Si^{3+} + Si^{4+}) = 502/641 = 0.8$

Based on the area values for each component and by taking into account the sensitivity factors, we calculated the ratio $Si^0/(Si^{1+} + Si^{2+} + Si^{3+} + Si^{4+})$ to be about 4/5 (or 45/55%) (see Table 3). With an average particle diameter of 20 nm, the Si^0 core corresponds to ca. 14 nm and the SiO_x passivating thickness of ca. 3 nm. When the oxygen associated with these suboxides is taken into account, the apparent value x for our Si/SiO_x nanoparticles is determined to be about 1.5.

High-energy nanomilling has been reported to lead to a certain degree of Si amorphization and pressure- or heat-induced crystallization.[49] This is of profound importance based on the increase in the extinction coefficient for amorphous Si vs crystalline Si.[14] Raman scattering has been used in both qualitative[30−32] and quantitative[33,34] studies to characterize thin films with polycrystalline and amorphous Si.[27,35] Raman shifts between 505 and 513 cm^{-1} for crystalline Si have been reported by Kamiya et al.[30] Iqbal and Veprek have shown that the peak frequency decreases from the single-crystal value of 520 cm^{-1} to 512 cm^{-1} for a crystallite size of 35 Å.[32] The starting material, a 325 mesh size polycrystalline Si powder (with 99.5% nominal purity) shows a typical Raman spectrum of microcrystalline Si (c-Si) with a peak at 512 ± 2 cm^{-1} with a fwhm of 12 ± 1 cm^{-1}, as determined by a Gaussian−Lorentzian fit (see Figure 3A). By subjecting this Si powder to high-energy milling, we obtained nanocrystalline particles that exhibit both amorphous (a-Si Raman line at 475 ± 2 cm^{-1} and a fwhm of 67 ± 1 cm^{-1}) and crystalline (c-Si peak at 518 ± 2 cm^{-1} with a fwhm of 14 ± 1 cm^{-1}) phases; see Figure 3B (as-milled powder). The corresponding self-assembled Si/SiO_x nanoparticles on gold substrates (Figure 3C) show similar features (i.e., a-Si Raman line with a peak at 480 ± 2 cm^{-1} with a fwhm of 69 ± 1 cm^{-1} and a c-Si peak at 519 ± 2 cm^{-1} with a fwhm of 12 ± 1 cm^{-1}). The structure and property relation for ball-milled Si has been well described by Shen et al.,[49] wherein the observed amorphization was explained based on two

(46) Keefer, K. D. *Structure and Growth of Silica Condensation Polymers*; Zeigler, J. M., Gordon-Fearon, F. W., Eds.; American Chemical Society: Washington, DC, 1990; Vol. 224.
(47) McNeiil, K. J.; DiCaprio, J. A.; Walsh, D. A.; Pratt, R. F. *J. Am. Chem. Soc.* **1980**, *102*, 1859.
(48) Niwano, M.; Kageyama, J.-I.; Kinashi, K.; Miyamoto, N. *J. Vac. Sci. Technol., A* **1994**, *12*, 465.
(49) Shen, T. D.; Koch, C. C.; McCormick, T. L.; Nemanich, R. J.; Huang, J. Y.; Huang, J. B. *J. Mater. Res.* **1995**, *10*, 139.

possible mechanisms (i.e., pressure-induced amorphization and crystallite-refinement-induced amorphization). The corresponding shift of the crystalline Raman line (starting from the as-received polycrystalline sample at 512 cm^{-1} to the as-milled Si at 518 cm^{-1}) is presently believed to be associated with increasing crystallite size[32] due to the heat generated during the high-energy milling process. Olego et al. proposed a model of the microcrystalline structure of annealed SiO_x semi-insulating polycrystalline silicon (SIPOS) films grown by low-pressure chemical vapor deposition. The Raman spectra of the self-assembled films of $Si/SiO_{1.5}$ nanoparticles lend further credibility to the amorphization process. According to Olego et al.[35] the atomic percent contribution of Si atoms to the ordered Si and disordered Si components can be quantified by assuming a direct relation between the deconvoluted areas for the crystalline and amorphous components.

Based on this model and the value of x, determined by XPS, we are able to estimate the relative percentages of amorphous and crystalline silicon. From the XPS data (see Figure 1), the atomic percent of Si atoms bonded to oxygen was found to be 55%. For both as-milled Si and self-assembled Si/SiO_x nanoparticles, the Si^0 content is 45%. The atomic percent contribution of Si to the crystalline and amorphous components for the as-milled Si is about 37 and 8%, respectively (Figure 3B). As a result of the subsequent sonication process, required for obtaining these Si/SiO_x suspensions, the crystalline component of these nanoparticles was reduced to 34% with a corresponding amorphous content of 11% (Figure 3C).

Conclusion

A systematic investigation into the chemistry and structure of nanosized silicon as-obtained via a high-energy ball milling process has been presented for the sonication-assisted formation of Si/SiO_x ethanolic suspensions. These Si/SiO_x suspensions that spontaneously assemble on glass surfaces were investigated as a function of pH in a variety of oxidizing agents and atmospheres. For pH below 5 and in the absence of H_2O, the Si−OEt groups present on the surface of these nanoparticles get protonated and are therefore attracted to a less positively charged glass substrate. XPS structure characterization is consistent with a core/shell (Si/SiO_x) nanoparticle structure with an average Si-atom ratio of 45/55 and $x \approx 1.5$. Raman characterization suggests that the Si core is composed of crystalline and amorphous parts with a respective ratio of 34 and 11 out of 45% of total Si atoms.

Acknowledgment. The authors would like to thank Dr. J. Chen and Prof. F. Jain for helpful discussions. Financial support from NSF, ECS 9528731, DMR-970220, and the Critical Technologies Program is greatly appreciated.

Supporting Information Available: Titration curve of Si/SiO_x nanoparticles between a pH regime of 8 and 4.5 (PDF). This material is available free of charge via the Internet at http://pubs.acs.org.

CM010362L